Glutathione is Required for Efficient Post-Golgi Trafficking of Incoming HPV16 Genome

Short title: Papillomavirus L2/vDNA Translocation Requires GSH

Shuaizhi Li[1], Matthew P. Bronnimann[1,§], Spencer J. Williams[2], and Samuel K. Campos[1,2,3,4*]

[1]Department of Immunobiology, University of Arizona, Tucson, AZ USA

[2]Department of Molecular & Cellular Biology, University of Arizona, Tucson, AZ USA

[3]Cancer Biology Graduate Interdisciplinary Program, University of Arizona, Tucson, AZ USA

[4]BIO5 Institute, University of Arizona, Tucson, AZ USA

*Corresponding Author: skcampos@email.arizona.edu

[§]Present affiliation: Roche Tissue Diagnostics, Tucson, AZ 85755

keywords: Papillomavirus, HPV, HPV16, Minor capsid protein, L2, glutathione, translocation

Abstract

Human papillomavirus (HPV) is the most common sexually transmitted pathogen in the United States, causing 99% of cervical cancers and 5% of all human cancers worldwide. HPV infection requires transport of the viral genome (vDNA) into the nucleus of basal keratinocytes. During this process, minor capsid protein L2 facilitates subcellular retrograde trafficking of the vDNA from endosomes to the Golgi, and accumulation at host chromosomes during mitosis for nuclear retention and localization during interphase. Here we investigated the relationship between cytosolic GSH and HPV16 infection. siRNA knockdown of GSH biosynthetic enzymes results in a partial decrease of HPV16 infection. Likewise, infection of HPV16 in GSH depleted keratinocytes is inefficient, an effect that was not seen with adenoviral vectors. Analysis of trafficking revealed no defects in cellular binding, entry, furin cleavage of L2, or retrograde trafficking of HPV16, but GSH depletion hindered post-Golgi trafficking and translocation, decreasing nuclear accumulation of vDNA. Although precise mechanisms have yet to be defined, this work suggests that GSH is required for a specific post-Golgi trafficking step in HPV16 infection.

Introduction

Human papillomavirus (HPV) is the most common sexually transmitted infection in the United States (1). Currently there are >300 HPV types that have been deposited and annotated in the Papillomavirus Episteme (PAVE) database (2). Based on disease association, HPV can be divided into low-risk HPV and cancer-associated high-risk HPV (3). Most HPVs are considered as low-risk HPV, causing cutaneous and mucosal warts

(4). However, 99% of cervical cancers and 5% of all human cancers worldwide are caused by high-risk HPV infection (5,6). HPV16 belongs to the high-risk HPV, and HPV16 alone is responsible for >50% cervical cancers (7). There are highly effective vaccines being used to prevent high-risk HPV infection, but the vaccine cannot protect against all types of high-risk HPV infection and the high cost prevents people from developing world to get access to the vaccine (7).

HPVs are small non-enveloped DNA viruses. The icosahedral capsid is built from 72 pentamers (360 molecules) of the major capsid protein L1. Within this particle, variable copies (<72 molecules but typically 20-40) of minor capsid protein L2 are complexed to the ~8kb dsDNA genome (vDNA). At the cellular level, HPV infection begins with virion attachment to keratinocytes via heparin sulfate proteoglycans (HSPGs) followed by furin- and kalleikrein- dependent cleavage of the capsid (8,9), likely causing conformational changes and transfer to secondary entry receptor complex(es). The nature of the entry complex(es) is still debatable but likely include growth factor receptor tyrosine kinases, integrins, tetraspanins, and annexin A2 (10,11). Asynchronous cellular uptake of virion occurs by macropinocytosis-like mechanisms after this potentially prolonged residence on the cell surface (12,13).

Internalized virions initially traffic through the endosomal compartment where low pH and the intramembrane protease complex γ-secretase trigger membrane insertion and protrusion of L2 through the vesicular membrane into the cytosol for recruitment of sorting nexins and retromer (14-18). A C-terminal charged region of L2, with inherent “cell penetration peptide” properties is also important for protrusion of L2 across the endosomal membranes (19). In this manner L2 dictates the retrograde trafficking of

L2/vDNA complexes from endosomes to the *trans*-Golgi network (TGN), an obligate step of initial infection (20,21). Membrane-bound vDNA, still in complex with L2, exits from the vesiculating TGN at the onset of mitosis and migrates towards metaphase chromosomes where L2 directly binds, tethering the vDNA to host chromosomes to ensure efficient nuclear delivery (22,23). As daughter cells return to G1, chromosomes decondense and PML bodies are recruited to the L2/vDNA, a process that appears to be necessary for efficient viral transcription (24,25).

HPV has evolved to infect and replicate in differentiating cutaneous or mucosal epithelium, and the viral life cycle is tightly intertwined with cellular differentiation of this tissue. Initially, HPV infects undifferentiated basal keratinocytes, resulting in low copy number maintenance of the episomal vDNA (3,26,27). Viral replication is achieved through the coordinated expression of viral early and late genes in response to cellular differentiation, resulting in vDNA amplification, expression of L1 and L2 capsid proteins, and assembly of progeny virions (3). Mature virions exist in an oxidized state, with intercapsomeric disulfide bonds stabilizing the particle by crosslinking of neighboring L1 pentamers (28-30). Pseudovirus particles generated through the 293TT system (31-33) must be “matured” in vitro to achieve this oxidized state but virions generated through organotypic raft cultures achieve this stabilized state through a naturally occuring redox gradient in the epithelial tissue where cells of the basal and suprabasal layers contain abundant free thiols and are in a reduced state relative to the upper cornified layers of the tissue (31,34).

Homeostasis of cellular thiol and disulfide redox is largely maintained by a large intracellular pool of glutathione (GSH). Given natural redox gradient of the epithelium,

and the prominent role of GSH in maintaining redox balance (35) we sought to investigate the role of cellular GSH in HPV16 infection. We find that siRNA knockdown of key enzymes in the GSH synthesis pathway impairs HPV16 pseudovirus infection. Depletion of the intracellular GSH pool caused a marked decrease in the infection of HPV16 but not adenoviral vectors. GSH was not important for HPV16 binding, endocytic uptake, cleavage of minor capsid protein L2, or trafficking of vDNA to the TGN, but was critical for efficient post-Golgi trafficking and intranuclear delivery of HPV16 L2/vDNA. Further work will be necessary to specifically define the GSH-dependent factors necessary for HPV16 infection.

Results

Knockdown of GSH biosynthesis enzymes partially blocks HPV16 infection.

Several enzymes are important in regulating GSH biosynthesis and maintaining a proper GSH(reduced)/GSSG(oxidized) ratio (Fig 1A) (36). Glutamate cysteine ligase (GCL, EC 6.3.2.2) is a rate-limiting enzyme in GSH biosynthesis pathway, responsible for generating the dipeptide γ-glutamylcysteine (γ-GC) from intracellular cysteine and glutamate (37). Glutathione synthetase (GSS, EC 6.3.2.3) then adds glycine to γ-GC, forming GSH (38). Cells normally maintain GSH at high concentrations, ranging from 1-10 mM. Such a high concentration of reduced GSH protects cells from oxidative stress and reactive oxygen species (ROS), through the actions of free GSH and GSH-dependent glutathione peroxidases and glutaredoxins (39,40). Glutathione reductase (GR, EC 1.8.1.7) maintains a high GSH/GSSG ratio by converting oxidized GSSG back

to two molecules of reduced GSH (41). This high concentration of reduced GSH maintains the cytosol in a reduced state, favoring free thiols over disulfides.

To understand whether GSH and a reducing cytosolic environment is important for HPV16 infection, we targeted the enzymes GCL, GSS and GR for siRNA knockdown and measured HPV16 infection in HaCaT cells. The heterodimeric enzyme GCL is comprised of two protein subunits; the catalytic GCLc and the modulatory GCLm (42). Maximal catalytic activity of GCL holoenzyme is only achieved upon binding of the modulatory GCLm to the catalytic GCLc subunit. GCLm is expressed at lower levels than GCLc, and is therefore rate-limiting in the formation of active GCL holoenzyme (43). Thus, we chose to target the GCLm subunit for siRNA knockdown experiments.

HPV16 infection dropped about 40-50% upon knockdown of either the modulatory subunit of GCL or GR (Fig.1B,C), suggesting that the cytosolic GSH may be important in facilitating the HPV16 infection. To our surprise, cells became slightly more permissive to HPV16 infection upon knockdown of GSS (Fig.1B,C). Previous research suggests that the intermediate thiol-containing metabolite γ-GC can substitute for GSH to help remove reactive oxygen species (44,45). The slight increase of the HPV16 infection in GSS knockdown cells may be due to substitution of γ-GC for GSH.

GSH is important for HPV16 to establish efficient infection.

To further verify importance of cytosolic glutathione in HPV16 infection, HaCaT cells were treated with L-buthionine-(S,R)-sulfoximine (BSO), an irreversible and specific transition-state inactivator of GCL (46), prior to HPV16 infection. As treatment with BSO only blocks nascent GSH synthesis, time is required for a drop in cytosolic

levels of GSH to be observed. After 72h treatment with 800μM BSO, cytosolic GSH levels were drastically depleted compared to the control vehicle-treated cells (Table 1). BSO treated HaCaT cells displayed a slightly slower proliferation rate and cell cycle anaylsis by PI staining revealed a subtle but statistically insignificant expansion of S phase upon BSO treatment (Fig 2A,B). This is consistent with other studies that BSO treatment does not considerably alter cell cycle kinetics (47,48). HPV16 infection levels dropped about 70% upon BSO treatment (Fig 2C), again suggesting that cytosolic GSH is required for efficient HPV16 infection. To rule out pleiotropic effects of BSO on luciferase expression, control or BSO treated HaCaT cells were infected with a luciferase-expressing ΔE1/E3 adenovirus (HAd5-Luc) and luciferase was measured 24h post infection. In this case, BSO actually enhanced HAd5-luc infection (Fig 2D), implying that the inhibition of HPV16 is not due to some non-specific effects of BSO on cellular viability, endocytosis, general transcription, or activity of the luciferase enzyme itself.

Effects of GSH depletion on viral binding, entry, and uncoating.

To determine the reason for inefficient HPV16 infection upon GSH depletion we performed binding and entry studies. We first investigated HPV16 binding to control or BSO treated HaCaT cells. Pre-chilled cells were infected with HPV16 for 1h at 4°C to prevent viral endocytosis (49) and unbound virus was extensively washed away. Some groups received an additional wash in PBS buffer at pH=10.75 to remove any cell-bound virus as previously reported (12). Cell lysates were then collected, and bound L1 was detected by non-reducing SDS-PAGE and western blot. Similar levels of full-length

disulfide-linked L1 dimers and trimers were observed in control or BSO treated samples that did not receive the high pH washes (Fig 3A,B), indicating that GSH depletion had no effect on HPV16 binding and the the high pH wash does indeed remove extracellular virus.

Next we investigated viral uptake by pre-binding HPV16 to cells followed by a 2h shift to 37°C to allow entry. After 2h cells were either processed for non-reducing L1 western blot or cleared of extracellular virus by high pH washing and returned to 37C for additional times. In this manner we are able to track the population of intracellular HPV16 that has entered the cells during the initial 2h incubation. Upon return to 37°C this “2h wave” of incoming virus will continue trafficking through the degradative endolysosomal system. Size shifts of L1 in western blots are thereby indicative of intracellular L1 cleavage and degradation during post-entry trafficking. Analysis of entry in this manner revealed no major differences between control and BSO treated HaCaT cells (Fig 3C). Both groups accumulated similar levels of high molecular weight (HMW) L1 within the initial 2h of uptake, and both groups showed similar kinetics of L1 degradation as evidenced by disappearance of the HMW L1 and concomitant appearance of the smaller 25 kDa L1 cleavage product.

Additional immunofluorescence and microscopy experiments were performed to investigate viral trafficking and disassembly within control and BSO treated cells. After HPV16 uptake, resident proteases within the acidic endosomal compartments promote the breakdown and disassembly of the L1 capsid. Although this degradative uncoating is not an obligate step of the infectious trafficking pathway, it does serve as a proxy for endolysosomal trafficking (8,50,51). Exposure of the L1-7 epitope, which is buried within

184 the intact capsid (52), is a useful marker for degradative uncoating and normally occurs
185 by 6-8h post infection (53). Control and BSO treated cells were infected with HPV16 for
186 2h or 8h and total L1 or L1-7 levels were visualized by immunofluorescence staining
187 and confocal microscopy. L1-7 was undetectable in either group at the early 2h time
188 point, as expected (Fig 3D). Both the control and BSO treated groups displayed
189 significant L1-7 signal by 8h, indicative of capsid degradation and proper endolysosomal
190 trafficking (Fig 3D). Taken together these data suggest GSH depletion does not
191 significantly affect HPV16 binding, entry, or early subcellular trafficking events.
192
193 **Depletion of GSH does not affect furin cleavage of L2.**
194 During HPV16 infection, the N-terminal 12 amino acids of L2 are removed by furin
195 cleavage (54), an obligatory step for proper retrograde trafficking and infection
196 (reviewed in (18)). To determine if BSO affects furin processing of L2 we utilized a
197 previously described system to easily monitor L2 cleavage called PSTCD-L2 (54). Since
198 a 12 amino acid difference is difficult to resolve by SDS-PAGE, the 70-residue
199 *Propionibacterium shermanii* transcarboxylase domain (PSTCD) is fused on the N-
200 terminus of L2 to generate a 9kDa size shift upon furin cleavage. Control or BSO
201 treated cells were infected with PSTCD-L2 virus and levels of L2 cleavage were
202 measured at 16h post infection by western blot of cell lysates and staining for total L2.
203 No significant differences were observed in the amount of cleaved L2 (Fig 3E),
204 indicating that cytosolic GSH does not affect furin processing of L2.
205
206 **GSH is important for L2/vDNA post-Golgi trafficking and translocation.**

HPV16 must transport its viral genome into the cell nucleus to successfully establish infection. This process involves trafficking of L2/vDNA from endolysosomal compartments to the *trans*-Golgi where upon mitosis post-Golgi vesicle-bound L2/vDNA tethers to mitotic chromosomes for nuclear localization and ultimately penetrates the limiting membrane to gain access to transcriptional machinery (22,23,55). To assess Golgi and nuclear localization of L2/vDNA, we infected control or BSO treated HaCaT cells with virions containing either EdU-labeled vDNA or L2-3xFlag. Cells were infected for 24h, surface virus was removed by high pH washing, and infection was continued for 8h prior to fixation, permeabilization, and staining. BSO (or water control) was included in the media for the duration of the infection. Cells were stained for either EdU (vDNA) or 3xFlag along with TGN46, a *trans*-Golgi marker. In some EdU staining experiments, p230 was used as the counterstain for the *trans*-Golgi. Nuclei were stained with DAPI. In control cells most of the EdU-labeled vDNA or L2-3xFlag was found overlapping with DAPI, within the cell nucleus (Fig 4A,B,C). In contrast, BSO treatment resulted in the retention of the vast majority of EdU labeled vDNA or L2-3xFlag within the *trans*-Golgi, as seen by overlap with either TGN46 or p230 (Fig 4A,B,C). Manders overlap coefficients (56) were measured from multiple Z-stacks across replicate experiments and differences were found to be statistically significant (Fig 4D). These data indicate that while L2/vDNA was efficiently transported to the *trans*-Golgi, GSH depletion prevented efficient exit from this compartment.

In prior work we developed a system to monitor translocation of L2 across limiting membranes (23). The platform is based on the C-terminal fusion of the biotin ligase BirA to L2. BirA will specifically biotinylate the BAP (biotin acceptor peptide)

substrate. Upon passage of L2-BirA across limiting membranes in reporter HaCaT-GFP-BAP cells, BirA will encounter and biotinylate the substrate GFP-BAP providing an easy readout for translocation. We first confirmed that the HaCaT-GFP-BAP cells were efficiently depleted for GSH upon treatment with BSO (Table 1) and that this led to inhibition of HPV16 infection as observed with parental HaCaT cells (Fig 5A). Translocation experiments with L2-BirA in control or BSO treated HaCaT-GFP-BAP cells revealed that GSH is required for efficient translocation across limiting membranes (Fig 5B,C), in agreement with the trafficking data (Fig 4). Taken together, cytosolic GSH is important for post-Golgi trafficking and translocation of L2-vDNA.

Discussion

Here we show that GSH is necessary for efficient infection by HPV16. siRNA knockdown of the GSH biosynthetic enzymes γ-GCS and GR blocked HPV16 infection by 40-50%. Conversely, knockdown of GSS, which results in the buildup of the thiol-containing metabolite γ -GC, caused a subtle increase in HPV16 infection. Likewise complete depletion of cytosolic GSH with BSO treatment blocked HPV16 infection by 70-80%, dependent on cell type. The same treatment increased transduction by HAdV5 vectors, suggesting a block specific to HPV16. GSH depletion had no effect on binding, endocytosis, furin cleavage of minor capsid protein L2, or subcellular endolysosomal trafficking of virions or retrograde trafficking of L2/vDNA to the *trans*-Golgi.

Factors that influence or control post-Golgi transport and translocation of HPV16 L2/vDNA remain largely uncharacterized. Upon entry into mitosis vesicular bound L2/vDNA is believed to emanate from the scattered mitotic Golgi and traffic along the

253 microtubule spindle towards centrioles *en route* to the mitotic chromosomes (23,55). By
254 metaphase, EdU labeled vDNA can be visualized bound to host chromosomes, via a
255 central chromatin binding region (22,23). Herein we show that cytosolic GSH is
256 necessary for efficient egress from the Golgi, and depletion of GSH by BSO treatment
257 inhibits HPV infection by preventing nuclear localization of L2/vDNA.

258 Although the precise mechanisms underlying the requirement for GSH remain to
259 be determined, these findings are novel and significant because they represent only the
260 second broad cellular "factor" necessary for this enigmatic process, the first being
261 mitosis itself. Cells devote energy to maintain a high intracellular concentration of GSH,
262 which largely serves as an antioxidant to protect cells from oxidative stress and ROS.
263 This occurs primarily in the form of GSH-dependent glutaredoxin enzymes, which use
264 GSH to reduce protein disulfides (57), and GSH-dependent glutathione oxidase and
265 peroxidase enzymes that catalyze the reduction of O_2 and H_2O_2 by GSH (58,59). Free
266 glutathione can also directly reduce oxidized disulfides (60). Glutathione reductase is an
267 NADPH-dependent enzyme that reduces oxidized GSSG into free GSH, maintaining a
268 high cytosolic GSH/GSSG ratio. This high GSH/GSSG ratio ensures a reducing
269 cytosolic redox potential, and most cytosolic sulfhydryl groups are present as free thiols
270 rather than oxidized disulfides. These free protein thiols are therefore maintained in the
271 reduced state and protected from harmful oxidants by excess GSH.

272 Proteins important for vesicular trafficking and vesicle fusion including N-
273 ethylmaleimide (NEM) sensitive factor (NSF) and soluble NSF-attachment proteins
274 (SNAPs) are known to be inactivated by oxidation of key cysteine residues (61,62). The
275 Ras, Rho/Rac, and Rab families of GTPases, key modulators of cellular signaling,

cytoskeletal dynamics, organelle membrane remodeling, and vesicular transport, contain various C-terminal cysteine motifs that must be isoprernylated for proper membrane localization and function (63,64). ADP-ribosylation factor 1 (Arf1), an important GTPase that modulates Golgi physiology and vesicular trafficking also contains a critical NEM-sensitive cysteine residue (65). Moreover, protein S-glutathionylation and S-nitrosylation can regulate many aspects of cellular physiology, including vesicular trafficking (66,67). Thus, it is conceivable that some critical aspects of particular vesicular trafficking pathways may require reduced cysteine residues for efficient function, and disturbing the natural GSH/GSSG couple may disrupt this trafficking. Given the complexity of vesicular trafficking and GSH physiology, elucidating the exact mechanisms through which GSH depletion affects post-Golgi trafficking of HPV16 may prove difficult.

It is interesting that the observed defect in HPV16 infection upon GSH depletion matches the phenotype of the recently described “Golgi retention” L2 mutants IVAL286AAAA, RR302/305AA, and RTR313AAA (22,68). These mutations within the chromatin binding region of L2 prevent efficient tethering of L2 to mitotic chromosomes resulting in accumulation of vesicle-bound L2/vDNA at the Golgi compartment rather than localizing to the nucleus (22). It may therefore be worthwhile to examine how free GSH may affect chromatin binding and localization of L2.

Materials & Methods:

Cells and viruses. HaCaTs (immortalized keratinocytes) (69) and HaCaT-GFP-BAP cells that stably express cytosolic GFP-BAP (23) were cultured in high-glucose cDMEM

media supplemented with 10% fetal bovine serum (FBS), and antibiotic/antimycotic (Ab/Am, Gibco #15240062). Additional 200 ng/mL puromycin was used for maintaining HaCaT-GFP-BAP cells. 293TT cells were cultured in high-glucose cDMEM media supplemented with 10% bovine growth serum (BGS), Ab/Am, and 165ug/ml hygromycin B. HPV16 PsV encapsidating the luciferase expression plasmid pGL3-basic were generated as previously described (70). Briefly, 293TT cells were co-transfected with a pXULL-derived plasmid expressing both L1 and L2, and Transfected cells were harvested at 48hrs post-transfection by trypsinization and pelleted/resuspended in PBS + 9.5 mM $MgCl_2$ at 100 μl/10 cm plate, followed by the addition of Brij58 to 0.35%, ammonium sulfate (pH=9.0) to 25 mM, Benzonase nuclease to 0.3%, and 20U/mL exonuclease V (Epicentre Plasmid-Safe ATP-dependent DNase) with overnight incubation at 37°C to promote maturation of capsids. After maturation, 0.17 volumes of 5M NaCl was added and lysates were 1x freeze/thawed at -80/37°C to further break apart cellular structures. Lysates were cleared by centrifugation at 3000x g and supernatants were loaded onto discontinuous CsCl gradients made from 4 ml light (1.25 g/ml) CsCl underlaid with 4 ml heavy (1.4 g/ml) CsCl. Virions were purified by 18h ultracentrifugation at 20,000 rpm at 4°C in Beckman SW41 Ti rotor/buckets. Viral bands were visible slightly above the gradient interface and were collected by side puncture with a 1.5” 18 gauge needle and 5 ml syringe. Virions were washed 3x and concentrated in VSB (25 mM HEPES pH 7.5, 0.5 M NaCl, 1 mM $MgCl_2$) using 100,000 MWCO centrifugation filter units (Millipore) and stored at -80°C. SYBR green qPCR was used to determine the packaged pGL3 copy number. The capsid/genome ratios were all within the normal range for typical HPV16 preps. To generate 5-ethynyl-2’-deoxyuridine

(EdU)-labeled virus, 15μM EdU was supplied in 293TT cell cultures before, during, and after the transfection of L1, L2 expressing plasmid and luciferase-expressing plasmid.

SDS-PAGE and western blotting. For denaturing/reducing polyacrylamide gel electrophoresis (PAGE), samples were lysed in either RLB (Reporter Lysis Buffer, Promega) or RIPA lysis buffer (50mM Tris-HCl PH=8.0, 150mM NaCl, 0.5 Na-deoxycholate, 0.5% SDS, supplemented with 1% PMSF and 1% protease inhibitor cocktail (Sigma P8340), combined with 20% total volume of denaturing/reducing SDS-PAGE buffer (contain 0.5M Tris, glycerol, 10%SDS, 2-mercaptoethanol and 1% bromophenol blue). Samples were then heated to 95°C for 5 minutes prior to separation on 10% or 12.5% polyacrylamide gels and run at 110V in gel running buffer (1X Tris-Glycine-SDS) for 90-105 minutes. Samples were transferred onto nitrocellulose membranes under 300mA for 75 minutes by using 1X Western transfer buffer (0.25M Tris, 1.92M Glycine) supplemented with 10% methanol. Membranes were blocked with 5% non-fat milk in 1XTBST (200mM Tris, 1.5M NaCl, 1% Tween20, pH=7.5) at 4°C overnight. For translocation experiments to detect GFP biotinylation, membranes were blocked in Odyssey Blocking Buffer TBS (LiCor) at 4°C overnight. For the denaturing/nonreducing PAGE, samples lysed by 1X RIPA lysis buffer supplemented with 1% PMSF, 1% proteinase inhibitor and 2mM N-ethylmaleimide (NEM) were mixed with 20% total volume of denaturing /non-reducing SDS-PAGE buffer (contain 0.5M Tris, glycerol, 10%SDS and 1% bromophenol blue). Samples were then incubated at room temperature for 10min prior to PAGE.

Western blot antibodies. Rabbit anti-GAPDH (Cell Signaling #2118) antibody was used at 1:5,000 dilution. Rabbit anti-GFP antibody (Clontech #632377) was used at 1:5,000 dilution. Mouse anti-L2 monoclonal K4-$L2_{20-38}$ (a kind gift from Martin Müller) antibody was diluted at 1:5,000. Mouse anti-GR (Santa Cruz #sc-133159) antibody was used at 1:50 dilution. Rabbit anti-GCLm (Santa Cruz #sc-22754) antibody was diluted 1:1,000. Mouse anti-GSS (Santa Cruz #sc-365863) antibody was diluted 1:250. Mouse anti-HPV16 L1 (Camvir-1) (Abcam #ab128817) antibody was used at 1:5,000. All the primary antibodies were diluted in 5% milk in TBST except K4-$L2_{20-38}$, which was diluted in 1% milk in TBST. All IR680- and IR800-conjugated secondary antibodies (Fisher Scientific PI35518, PISA535521, PI35568, PISA535571) were diluted 1:10,000 in 5% milk in TBST. For translocation experiments, NeutrAvidin Dylight 800-conjugate (Thermo #22853) was used at 1:10,000 dilution in LiCor blocking buffer. Blots were imaged on the Licor Odyssey Infrared Imaging System.

siRNA knockdown. HaCaT cells were seeded at 35,000 cells per well in 1ml siRNA media (high-glucose cDMEM supplemented with 10% FBS, antibiotic-free) in a 24 well plate. Prior to transfection, media was changed to 500ul per well Opti-MEM reduced serum medium with HEPES 2.4g/L sodium bicarbonate and L-glutamine (Gibco #31985070). Scramble control siRNA-A (sc-37007), GCLm (sc-40602), GR (sc-35505), and GSS (sc-41980), was diluted into Opti-MEM containing Lipofectamine RNAiMAX (Invitrogen #13778150) according to the manufacturer's instructions. 100μl per well siRNA-Lipofectamine complex (50 nM siRNA final) was added drop-wise to cells. At 16h

367 post-transfection, cells were washed with PBS and media was replaced with siRNA
368 media for 24h prior to viral infection assays.
369
370 **BSO treatment and infection assay.** L-Buthionine-(S, R)-sulfoximine (BSO, Santa
371 Cruz, CAS 83730-53-4) was prepared at 200 mM in water. Cells were pretreated with
372 800μM BSO for 72h prior to experiments. 50,000 cells/well of water or BSO-treated
373 HaCaTs were seeded in 24-well plate the day before infection. Cells were infected with
374 HPV16 at 2 x 10^8 viral genome equivalents (pGL3 copies) per well or 10,000 luciferase
375 expressing HAdV-5 vector particles per cell. At 24h post-infection, cells were lysed in
376 100μl RLB. 100μl luciferase assay reagent (Promega) was added into 20μl cell lysate
377 and luciferase activity was measured using a DTX800 Multimode plate reader
378 (Beckman Coulter). The remainder of the cell lysate was collected for western blots and
379 GAPDH immunostaining. GAPDH bands were quantified by densitometry using ImageJ
380 software (71) to normalize the luciferase data.
381
382 **Glutathione measurements.** GSH/GSSG-Glo assay kit (Promega, Cat.V6611) was
383 used for glutathione measurements. After 48h 800μM H_2O or BSO pretreatment, 10,000
384 H_2O-treated HaCaTs cells/per well or 15,000 BSO-treated cells/per well were
385 transferred into white 96 well plates. Then, another 24h H_2O or 800μM BSO treatment
386 was followed. To measure total GSH levels, 50ul per well total glutathione lysis reagent
387 (containing Luciferin-NT, passive lysis buffer) was added to the cells. To measure
388 oxidized GSSG, 50ul per well oxidized lysis reagent (containing Luciferin-NT, passive
389 lysis buffer, and 25mM NEM) was added. Plates were incubated at room temperature

and shaken for 5 minutes, then 50μl per well luciferin generation reagent (containing 100mM DTT, glutathione S-transferase and GSH reaction buffer) was added. The plate was shaken and incubated at room temperature for another 30 minutes. Finally, 100μl per well luciferin detection reagent was added and the plate was shaken and incubated at room temperature for another 15 minutes. The luminescence was measured using a DTX-800 multimode plate reader (Beckman Coulter). Standard curves were generated using serial dilutions of standard GSH (provided by the kit) ranging from 16uM to 0.25uM.

Binding and entry assays. BSO or H_2O treated cells were incubated on ice for 20 minutes before infecting with 1 μgL1/ml of HPV16 in cold cDMEM media supplemented with 10% FBS. Plates were kept on ice for 1h to allow viral particles to bind to the cell surface. For the binding experiments, cells were washed with cold PBS (pH=7.4) to completely remove the virus from the media. The control groups were washed with cold high-pH PBS (pH=10.75) followed by regular cold PBS to remove surface bound virus. Lysates were then collected for non-reducing SDS-PAGE. For entry experiments, cells were washed with PBS, replaced with fresh media, and incubated at 37°C in 5% CO_2 incubator after 1h virion pre-binding. After 2-hour incubation, cells were washed with high-pH PBS to remove the surface-bound virus and replaced with fresh media and incubated at 37°C. Samples were collected at the indicated times and processed for non-reducing SDS-PAGE.

412 **Furin cleavage experiments.** HaCaTs cells were pretreated with either 800 μM BSO or
413 H_2O as described above. After 48h pretreatment, 90,000/well of treated cells were
414 seeded on 12well plates followed by another 24h of BSO/H_2O treatment. Cells were
415 then infected with 800 ng of L1 per well of HPV16 virions containing the PSTCD-L2
416 fusion (54). At 16h post-infection, samples were lysed with RIPA lysis buffer
417 supplemented with 1% PMSF, 1% proteinase inhibitor and 20% denaturing reducing
418 SDS loading buffer. Western blot was performed as previously described. The intensity
419 of the uncleaved band and the cleaved band were quantified by densitometry using
420 ImageJ software (71) and the fraction of cleaved L2 was calculated.
421
422 **Immunofluorescence staining.** 100,000 cells/well of H_2O or BSO treated HaCaTs
423 cells were plated on coverslips in 6-well plates. Cells were infected with 500ng L1/ml of
424 virus. At 2h and 8h post-infection, cells were fixed with 2% formaldehyde (pH=7.4,
425 Fisher Scientific), permeabilized by 0.25% Triton X-100 (Fisher Scientific) and blocked
426 by using blocking solution (PBS plus 4% Bovine serum albumin, fraction V (Fisher
427 Scientific) supplemented with 1% goat serum). Rabbit anti-HPV16 polyclonal antibody
428 (a kind gift from M. Ozbun) was used at 1:1,000 dilution and mouse anti-L1-7 antibody
429 was used at 1:50 dilution. Cells were incubated with primary antibody at room
430 temperature for 1h, followed by 1h room temperature incubation of secondary goat anti-
431 mouse AlexaFluor-555 antibodies (1:1,000 dilution) and goat anti-rabbit 488 antibodies.
432 All antibodies were diluted in regular PBS contain 20% blocking solution. Prolong
433 diamond anti-fade mounting medium with DAPI (Life Technologies) were used for
434 mounting coverslips. For EdU experiments, Cells were infected with 1μg L1/ml of EdU

435 labeled HPV16 for 20h. Then, cells were washed and replaced with fresh media for
436 another 8h incubation. Cells were then washed with high-pH PBS (pH=10.75) followed
437 by regular PBS to remove all the surface-bound virus. Cells were then fixed,
438 permeabilized, and blocked as described above. Click-iT EdU AlexaFluor-488 kit
439 (Molecular Probes, Life Technologies #) was used for labeling the EdU according to the
440 manufacturer's protocol. Primary antibody and secondary antibody incubation were then
441 performed as described above. Rabbit anti-TGN46 (Sigma-Aldrich T7576) antibody was
442 used at 1:200 dilution. Mouse anti-p230 (BD Transduction Laboratories, #611280) was
443 used at 1:400 dilution. Goat anti-Rabbit AlexaFluor-555 secondary antibody was used at
444 1:1,000 dilution.
445
446 **Confocal microscopy.** Confocal microscopy was performed using a Zeiss LSM510
447 META system or the Zeiss LSM880 system with 405 nm, 488 nm, and 543 nm lasers.
448 Samples were examined using a 63x objective, and Z-stacks with a 0.35μm depth per
449 plane were taken of each image. Representative single-plane images were processed
450 with the Zeiss META software or Zen Blue software and further processed with ImageJ
451 software (71).
452
453 **Colocalization analysis.** Manders overlap coefficients (56) for a variety of channels
454 within individual Z-stacks were determined using the JACoP plugin (72) on ImageJ.
455 Thresholds were manually set below saturation. Individual Manders coefficient values
456 and mean values from multiple Z-stacks (each containing multiple cells), across 2-5
457 independent experiments, were plotted with GraphPad Prism software. p-values were

458 calculated with Prism using a two-sample unpaired *t*-test as recommended for
459 colocalization analysis (73).
460
461 **Translocation experiments.** 60,000 cells/well of H_2O or BSO treated HaCaT-GFP-BAP
462 cells were seeded in 24-well plate. Cells were infected with 150ng L1/well of HPV16 L2-
463 BirA virus (23). At 24h post-infection, samples were processed for reducing SDS-PAGE
464 followed by western blot to detect total and biotinylated GFP.
465
466 **PI staining and flow cytometry.** H_2O or BSO treated HaCaTs cells were trypsinized
467 and pelleted. The cell pellet was washed and resuspended in cold 70% ethanol. Cells
468 were then pelleted again and resuspended in 500ul cold PBS. Samples were incubated
469 at 37°C for 30 minutes under 1/20 volume of RNase A at 20mg/ml in TE buffer (50 mM
470 Tris-HCl (pH 8.0), 10 mM EDTA, and 1/40 volume of 1.6mg/ml propidium iodide.
471 Samples were analyzed on a BD Biosciences FACSCanto II flow cytometer using Diva
472 8.0 software. Counts for G1, S, or G2/M phases were plotted as percentages of cell
473 count on MS Excel.
474
475 **Statistics.** p-values were calculated with the appropriate two-sample paired or unpaired
476 *t*-tests using MS Excel or GraphPad Prism software, as indicated. A significance
477 threshold value of $p<0.05$ was applied.
478
479 **Acknowledgements.**
480 This work was supported by grant 1R01AI108751-01 from the National Institute for

Allergy and Infectious Diseases. We are grateful to Dr. Martin Müller for the K4-$L2_{20-38}$ monoclonal antibody, Dr. Martin Sapp for the L1-7 monoclonal antibody, Dr. Michelle Ozbun for the anti-HPV16 polyclonal antibody, Dr. Michael Barry for the HAdV5 vector, Dr. Chris Buck for the 293TT and Dr. Anne Cress for the HaCaT cells. We thank Patty Jansma of the UA ORD Imaging Core-Marley, and Paula Campbell and John Fitch of the UACC/ARL Cytometry Core Facility, which is funded by a UA Cancer Center Support Grant (CCSG - CA 023074).

Author Contributions

SKC and SL designed and conceived the experiments. SL, MBP, and SJW performed the experiments and analyzed the data. SKC and SL wrote the paper.

Table 1. Measurement of GSH concentrations in cells ± BSO.

Cell type/condition	[GSH]*	[GSSG]*	GSH/GSSG
HaCaT + H_2O	7.338 ± 1.19	0.093 ± 0.008	78.9
HaCaT + BSO	0.027 ± 0.006	N.D.	----
HaCaT-GFP-BAP + H_2O	7.652 ± 1.26	0.104 ± 0.01	73.6
HaCaT-GFP-BAP + BSO	0.025 ± 0.005	N.D.	----

*mean [μM] ±SEM, n=2 independent experiments. N.D = not determined, under the limit of detection.

Figures & Legends

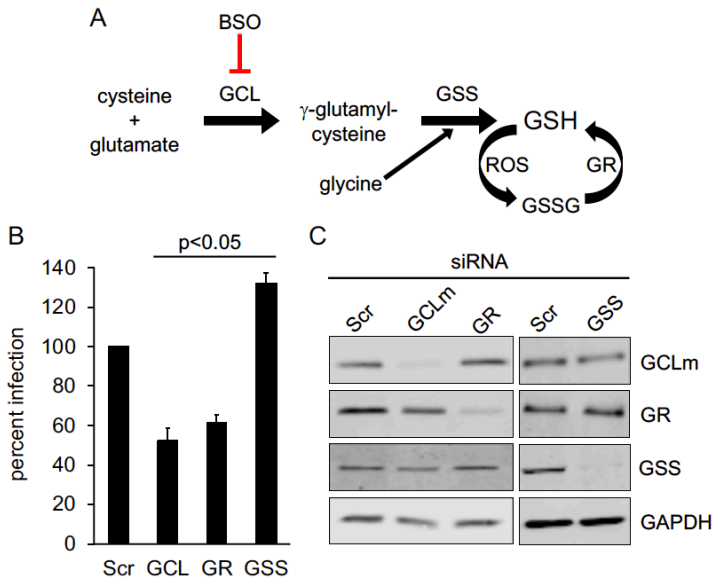

Fig 1. siRNA knockdown of GSH biosynthetic enzymes. (A) Schematic of GSH biosynthesis pathway. GCL catalyzes the ligation of cysteine and glutamate to generate γ-GC. Glycine is then added to γ-GC by GSS to form GSH, which can reduce ROS to form oxidized GSSG. GR maintains high levels of GSH by reducing GSSG back to GSH. BSO specifically blocks GCL, the rate-limiting enzyme in GSH biosynthesis pathway. **(B)** Infectivity of luciferase-expressing HPV16 in siRNA treated HaCaT cells. Cells were transfected with SCR, GCLm, GR or GSS siRNA for 18h prior to infection. Luciferase assays were performed 24h post infection and normalized to GAPDH expression level. The graph shows mean percent infection (±SEM, n=3 independent experiments) with Scr infection levels set to 100%. P-values were determined with a two-sample paired t-test. **(C)** Western blot to verify specific siRNA knockdown of GCLm, GR, and GSS.

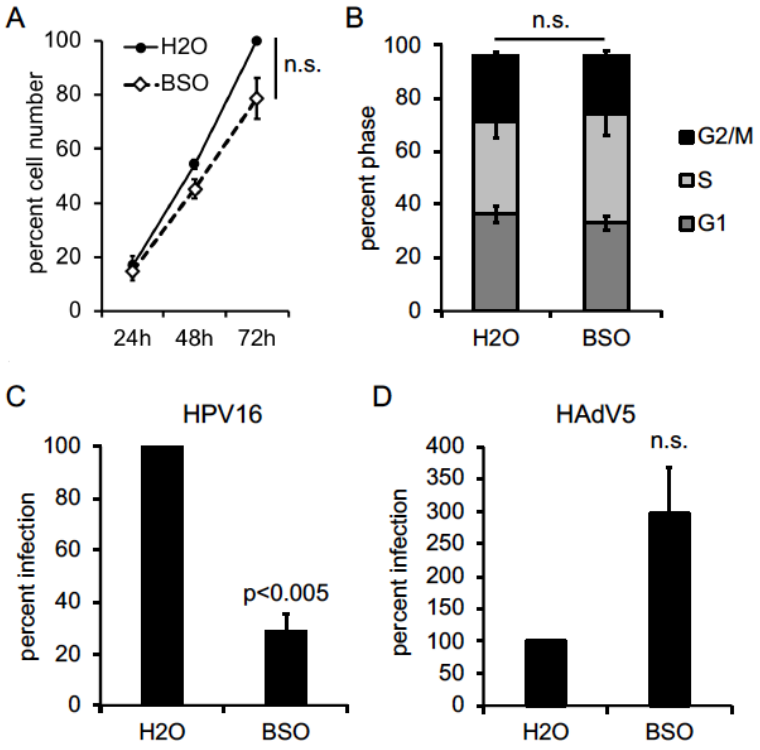

Fig 2. GSH is important for efficient HPV16 infection. (A) Growth curve of HaCaT cells ± BSO. The mean percent total number of cells is shown (±SEM, n=3 independent experiments). The 72h H_2O treated group was set to 100. **(B)** Cell cycle progression analysis in H_2O and BSO treated HaCaT cells, as measured by PI staining and flow cytometry. The graph shows the mean percent cell counts in G1, S, or G2/M phases (±SEM, n=3 independent experiments). **(C, D)** Infectivity of luciferase-expressing HPV16 **(C)** or luciferase-expressing HAdv5 **(D)** in HaCaT cells ± BSO. Luciferase assays were performed 24h post infection and data were normalized to GAPDH expression levels. The graph shows mean percent infection (±SEM), relative to H_2O treated cells, n=4 for **(C)**, n=3 for panel **(D)**. P-values were determined with a two-sample paired *t*-test, with significance cut off value set to p=0.05.

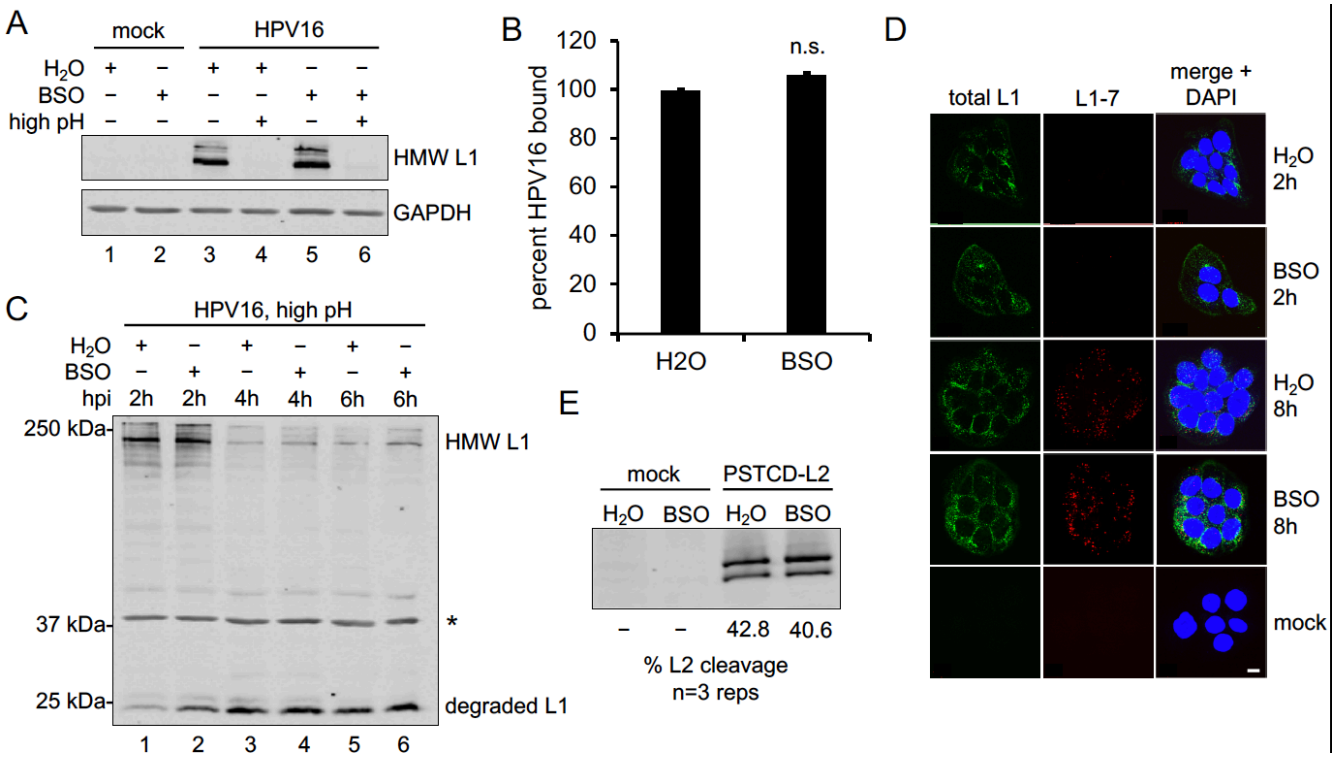

Fig 3. GSH depletion does not perturb early events of HPV16 infection. (A) Binding assay. HPV16 was bound to HaCaT cells ± BSO for 1hr at 4°C. Cells were washed with regular PBS (pH=7.2, lanes 1, 2, 3, and 5) or high pH PBS (pH=10.75, lanes 4 and 6) to remove the surface-bound virus before detection of cell-bound L1 by non-reducing SDS-PAGE and western blot. **(B)** Densitometric quantification of band intensities from binding assays. The graph shows mean percent L1 band intensity (±SEM, n=2 independent experiments) relative to the control group. P-values were determined with a two-sample paired *t*-test, with significance cut off value set to p=0.05. **(C)** HPV16 uptake assay. HaCaT cells ± BSO were prebound with virus and incubated for 2h at 37°C, at which time cell surface virus was removed by high pH PBS wash. Media ± BSO was replaced and infected cells were incubated at 37°C for additional times (4h and 6h total) to allow trafficking of intracellular virus. Cell lysates were processed for nonreducing SDS-PAGE and western blot to detect intact and degraded forms of L1.

*Asterisk marks a cellular protein that cross-reacts with the L1 antibody, and serves as an internal loading control. **(D)** Intracellular uncoating and degradation of HPV16 capsid. HaCaT cells ± BSO were plated on coverslips and infected with HPV16 for 2h or 8h prior to fixation and processing for IF as described in *Materials & Methods.* Total L1 was stained with rabbit anti-L1 polyclonal antibody and anti-rabbit secondary antibody (green). Degraded L1 was stained with mouse L1-7 monoclonal antibody and anti-mouse secondary antibody (red). Nuclei were stained with DAPI (blue). Representative micrographs are shown, scale bars = 10 μm. **(E)** L2 furin cleavage assay. HaCaT cells ± BSO were infected with PSTCD-L2 virus for 16h prior to SDS-PAGE and western blotting. L2 band intensities were quantified by densitometry using ImageJ and percent L2 cleavage was calculated from three biological repeats.

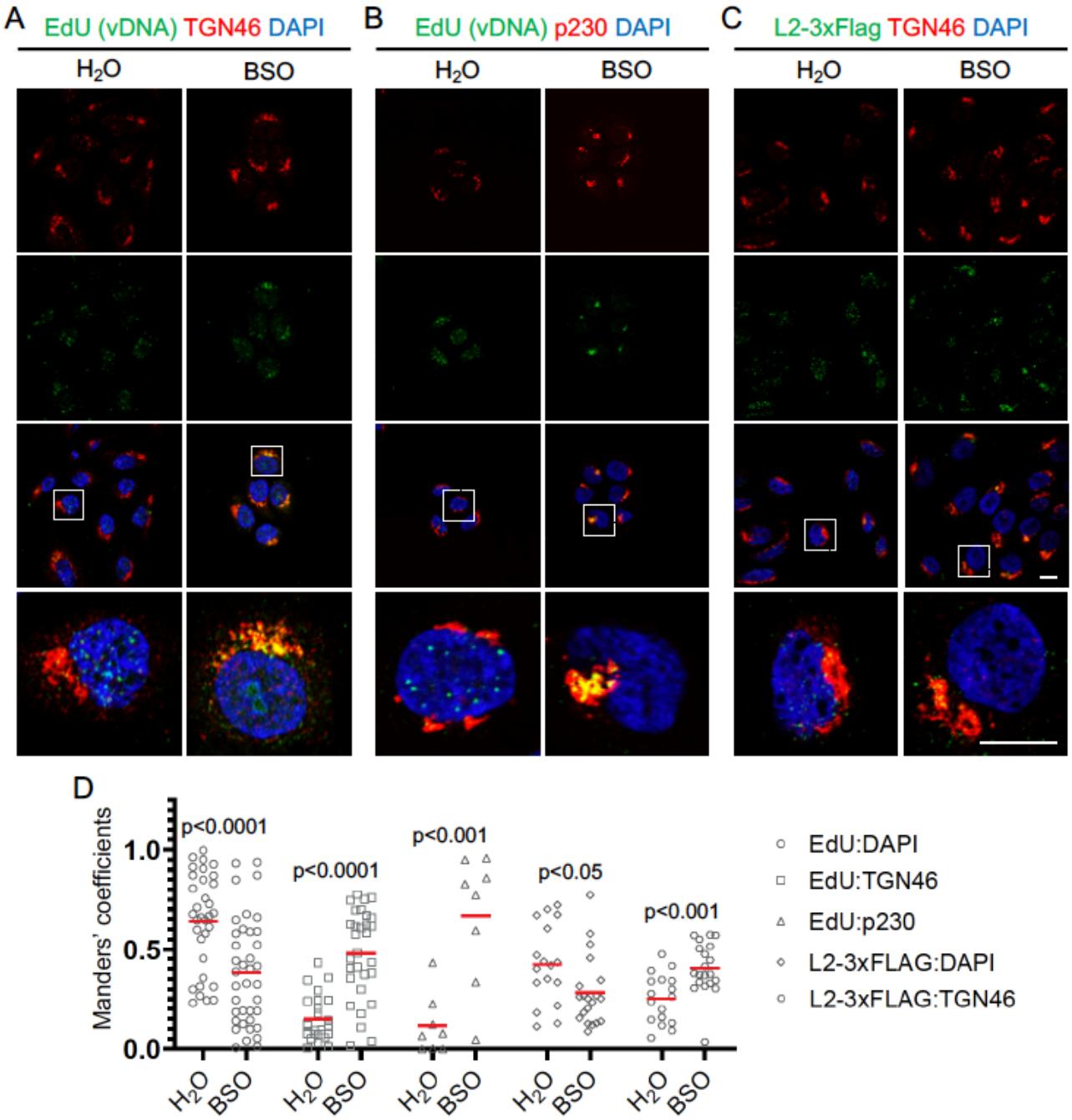

563

564

565 **Fig 4. Efficient L2/vDNA post-Golgi trafficking requires GSH. (A-C)** HaCaT cells ±

566 BSO were infected with HPV16 containing either EdU-labeled vDNA or L2-3xFlag for

567 24h at 37°C, followed by a high pH wash to remove surface virus, replacement of media

568 ± BSO, and incubation at 37°C for an additional 8h prior to fixation and processing for IF
569 staining as described in *Materials & Methods*. **(A)** Cells were stained with rabbit anti-
570 TGN46 with AlexaFluor-555 conjugated anti-rabbit secondary (red), and EdU-labeled
571 vDNA was stained with Click-iT EdU AlexaFluor-488 (green). **(B)** Cells were stained
572 with mouse anti-p230 antibody with AlexaFluor-555 conjugated anti-mouse secondary
573 (red), and EdU-labeled vDNA was stained with Click-iT EdU AlexaFluor-488 (green). **(C)**
574 Cells were stained with both mouse anti-FLAG antibody with AlexaFluor-488 conjugated
575 anti-mouse secondary (green), and AlexaFluor-555 conjugated anti-rabbit secondary
576 (red). For all panels cell nuclei were stained with DAPI (blue). Representative
577 micrographs are shown, scale bars = 10 μm. **(D)** Colocalization analysis of microscopy
578 data using the JACoP plugin of ImageJ. Manders overlap coefficients were measured
579 between EdU:DAPI, EdU:TGN46, EdU:p230, L2-3xFlag:DAPI, and L2-3xFlag:TGN46
580 for multiple Z-stacks, each containing multiple cells/field, from 2-5 independent
581 experiments. Red bars represent the mean Manders coefficient for each data set, data
582 points represent the Manders coefficient for each individual Z-stack. p-values were
583 determined with a two-sample unpaired *t*-test.
584
585
586
587
588
589
590

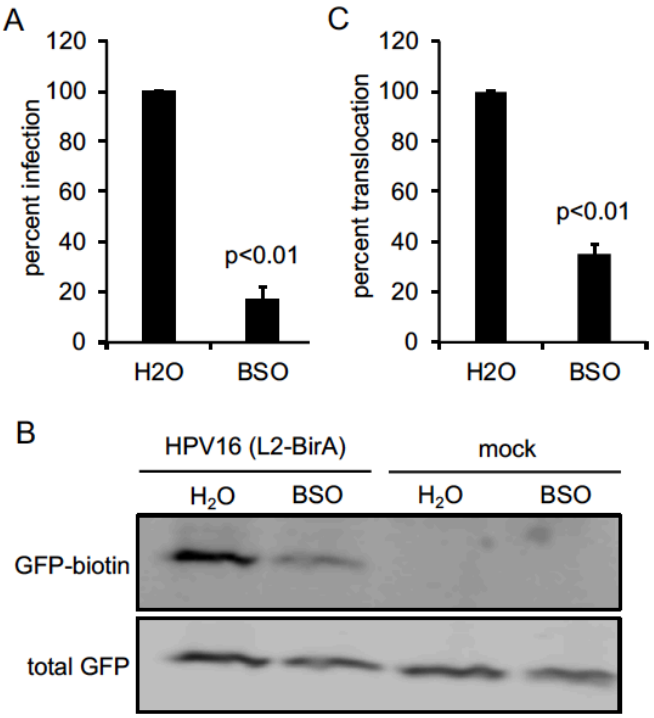

Fig 5. GSH is required for efficient L2/vDNA translocation. (A) Infectivity of HPV16 in HaCaT-GFP-BAP cells ± BSO. Luciferase assays were performed 24h post infection and data were normalized to GAPDH expression levels. The graph shows mean percent infection (±SEM, n=3 independent experiments), relative to H_2O treated cells. **(B)** Translocation assay. HaCaT-GFP-BAP cells ± BSO were infected with HPV16 containing L2-BirA. Biotinylation of GFP-BAP, a proxy for translocation across limiting membranes, was measured by SDS-PAGE and blotting with NeutrAvidin Dylight-800 conjugate. Total GFP was detected with rabbit anti-GFP antibody. **(C)** Quantification of the translocation assay blots. Band intensiies were measured by densitometry using ImageJ. The graph represents the mean percent biotin-GFP (±SEM, n=6 independent experiments), normalized to total GFP band intensity, and relative to the H_2O treated control group. For panels **(A, C)**, p-values were calculated with a two-sample paired *t*-test.

References.

1. Braaten, K. P., and Laufer, M. R. (2008) Human Papillomavirus (HPV), HPV-Related Disease, and the HPV Vaccine. *Reviews in Obstetrics and Gynecology* **1**, 2-10
2. Van Doorslaer, K., Li, Z., Xirasagar, S., Maes, P., Kaminsky, D., Liou, D., Sun, Q., Kaur, R., Huyen, Y., and McBride, A. A. (2017) The Papillomavirus Episteme: a major update to the papillomavirus sequence database. *Nucleic acids research* **45**, D499-D506
3. Doorbar, J., Quint, W., Banks, L., Bravo, I. G., Stoler, M., Broker, T. R., and Stanley, M. A. (2012) The biology and life-cycle of human papillomaviruses. *Vaccine* **30 Suppl 5**, F55-70
4. Doorbar, J. (2016) Model systems of human papillomavirus-associated disease. *J Pathol* **238**, 166-179
5. Walboomers, J. M., Jacobs, M. V., Manos, M. M., Bosch, F. X., Kummer, J. A., Shah, K. V., Snijders, P. J., Peto, J., Meijer, C. J., and Muñoz, N. (1999) Human papillomavirus ia a necessary cause of invasive cervical cancer worldwide. *J Pathol* **189**, 12-19
6. zur Hausen, H. (2002) Papillomaviruses and cancer: from basic studies to clinical application. *Nat Rev Cancer* **2**, 342-350
7. Forman, D., de Martel, C., Lacey, C. J., Soerjomataram, I., Lortet-Tieulent, J., Bruni, L., Vignat, J., Ferlay, J., Bray, F., Plummer, M., and Franceschi, S. (2012) Global burden of human papillomavirus and related diseases. *Vaccine* **30 Suppl 5**, F12-23
8. Cerqueira, C., Samperio Ventayol, P., Vogeley, C., and Schelhaas, M. (2015) Kallikrein-8 Proteolytically Processes Human Papillomaviruses in the Extracellular Space To Facilitate Entry into Host Cells. *J Virol* **89**, 7038-7052
9. Richards, R. M., Lowy, D. R., Schiller, J. T., and Day, P. M. (2006) Cleavage of the papillomavirus minor capsid protein, L2, at a furin consensus site is necessary for infection. *Proc Natl Acad Sci U S A* **103**, 1522-1527
10. Mikulicic, S., and Florin, L. (2019) The endocytic trafficking pathway of oncogenic papillomaviruses. *Papillomavirus research* **7**, 135-137
11. Ozbun, M. A. (2019) Extracellular events impacting human papillomavirus infections: Epithelial wounding to cell signaling involved in virus entry. *Papillomavirus research* **7**, 188-192
12. Schelhaas, M., Shah, B., Holzer, M., Blattmann, P., Kühling, L., Day, P. M., Schiller, J. T., and Helenius, A. (2012) Entry of Human Papillomavirus Type 16 by Actin-Dependent, Clathrin- and Lipid Raft-Independent Endocytosis. *PLoS Pathogens* **8**, e1002657
13. Becker, M., Greune, L., Schmidt, M. A., and Schelhaas, M. (2018) Extracellular conformational changes in the capsid of human papillomaviruses contribute to asynchronous uptake into host cells. *J Virol*
14. Inoue, T., Zhang, P., Zhang, W., Goodner-Bingham, K., Dupzyk, A., DiMaio, D., and Tsai, B. (2018) gamma-Secretase promotes membrane insertion of the human papillomavirus L2 capsid protein during virus infection. *J Cell Biol* **217**, 3545-3559

15. Zhang, W., Kazakov, T., Popa, A., and DiMaio, D. (2014) Vesicular trafficking of incoming human papillomavirus 16 to the Golgi apparatus and endoplasmic reticulum requires gamma-secretase activity. *mBio* **5**, e01777-01714
16. Popa, A., Zhang, W., Harrison, M. S., Goodner, K., Kazakov, T., Goodwin, E. C., Lipovsky, A., Burd, C. G., and DiMaio, D. (2015) Direct binding of retromer to human papillomavirus type 16 minor capsid protein L2 mediates endosome exit during viral infection. *PLoS Pathog* **11**, e1004699
17. Bergant Marusic, M., Ozbun, M. A., Campos, S. K., Myers, M. P., and Banks, L. (2012) Human papillomavirus L2 facilitates viral escape from late endosomes via sorting nexin 17. *Traffic* **13**, 455-467
18. Campos, S. K. (2017) Subcellular Trafficking of the Papillomavirus Genome during Initial Infection: The Remarkable Abilities of Minor Capsid Protein L2. *Viruses* **9**
19. Zhang, P., Monteiro da Silva, G., Deatherage, C., Burd, C., and DiMaio, D. (2018) Cell-Penetrating Peptide Mediates Intracellular Membrane Passage of Human Papillomavirus L2 Protein to Trigger Retrograde Trafficking. *Cell* **174**, 1465-1476 e1413
20. Day, P. M., Thompson, C. D., Schowalter, R. M., Lowy, D. R., and Schiller, J. T. (2013) Identification of a role for the trans-Golgi network in human papillomavirus 16 pseudovirus infection. *J Virol* **87**, 3862-3870
21. Lipovsky, A., Popa, A., Pimienta, G., Wyler, M., Bhan, A., Kuruvilla, L., Guie, M.-A., Poffenberger, A. C., Nelson, C. D. S., Atwood, W. J., and DiMaio, D. (2013) Genome-wide siRNA screen identifies the retromer as a cellular entry factor for human papillomavirus. *Proceedings of the National Academy of Sciences of the United States of America* **110**, 7452-7457
22. Aydin, I., Villalonga-Planells, R., Greune, L., Bronnimann, M. P., Calton, C. M., Becker, M. A., Lai, K. Y., Campos, S. K., Schmidt, and Schelhaas, M. A. (2017) A central region in the minor capsid protein of papillomaviruses facilitates viral genome tethering and membrane penetration for mitotic nuclear entry.
23. Calton, C. M., Bronnimann, M. P., Manson, A. R., Li, S., Chapman, J. A., Suarez-Berumen, M., Williamson, T. R., Molugu, S. K., Bernal, R. A., and Campos, S. K. (2017) Translocation of the papillomavirus L2/vDNA complex across the limiting membrane requires the onset of mitosis.
24. Day, P. M., Baker, C. C., Lowy, D. R., and Schiller, J. T. (2004) Establishment of papillomavirus infection is enhanced by promyelocytic leukemia protein (PML) expression. *Proc Natl Acad Sci U S A* **101**, 14252-14257
25. Guion, L., Bienkowska-Haba, M., DiGiuseppe, S., Florin, L., and Sapp, M. (2019) PML nuclear body-residing proteins sequentially associate with HPV genome after infectious nuclear delivery. *PLoS Pathog* **15**, e1007590
26. Longworth, M. S., and Laimins, L. A. (2004) Pathogenesis of human papillomaviruses in differentiating epithelia. *Microbiol Mol Biol Rev* **68**, 362-372
27. Schiffman, M., Doorbar, J., Wentzensen, N., de Sanjose, S., Fakhry, C., Monk, B. J., Stanley, M. A., and Franceschi, S. (2016) Carcinogenic human papillomavirus infection. *Nature reviews. Disease primers* **2**, 16086
28. Buck, C. B., Day, P. M., and Trus, B. L. (2013) The papillomavirus major capsid protein L1. *Virology* **445**, 169-174

29. Buck, C. B., Thompson, C. D., Pang, Y. Y., Lowy, D. R., and Schiller, J. T. (2005) Maturation of papillomavirus capsids. *J Virol* **79**, 2839-2846
30. Cardone, G., Moyer, A. L., Cheng, N., Thompson, C. D., Dvoretzky, I., Lowy, D. R., Schiller, J. T., Steven, A. C., Buck, C. B., and Trus, B. L. (2014) Maturation of the human papillomavirus 16 capsid. *mBio* **5**, e01104-01114
31. Biryukov, J., and Meyers, C. (2015) Papillomavirus Infectious Pathways: A Comparison of Systems. *Viruses* **7**, 4303-4325
32. Buck, C. B., Pastrana, D. V., Lowy, D. R., and Schiller, J. T. (2005) Generation of HPV pseudovirions using transfection and their use in neutralization assays. *Methods in molecular medicine* **119**, 445-462
33. Pyeon, D., Lambert, P. F., and Ahlquist, P. (2005) Production of infectious human papillomavirus independently of viral replication and epithelial cell differentiation. *Proc Natl Acad Sci U S A* **102**, 9311-9316
34. Conway, M. J., Alam, S., Ryndock, E. J., Cruz, L., Christensen, N. D., Roden, R. B., and Meyers, C. (2009) Tissue-spanning redox gradient-dependent assembly of native human papillomavirus type 16 virions. *J Virol* **83**, 10515-10526
35. Meister, A. (1995) Glutathione metabolism. *Methods in enzymology* **251**, 3-7
36. Meister, A. (1988) Glutathione metabolism and its selective modification. *The Journal of biological chemistry* **263**, 17205-17208
37. Wild, A. C., and Mulcahy, R. T. (2000) Regulation of gamma-glutamylcysteine synthetase subunit gene expression: insights into transcriptional control of antioxidant defenses. *Free radical research* **32**, 281-301
38. Njalsson, R., and Norgren, S. (2005) Physiological and pathological aspects of GSH metabolism. *Acta paediatrica (Oslo, Norway : 1992)* **94**, 132-137
39. Arthur, J. R. (2000) The glutathione peroxidases. *Cellular and molecular life sciences : CMLS* **57**, 1825-1835
40. Xiao, Z., La Fontaine, S., Bush, A. I., and Wedd, A. G. (2019) Molecular Mechanisms of Glutaredoxin Enzymes: Versatile Hubs for Thiol-Disulfide Exchange between Protein Thiols and Glutathione. *Journal of molecular biology* **431**, 158-177
41. Zhao, Y., Seefeldt, T., Chen, W., Wang, X., Matthees, D., Hu, Y., and Guan, X. (2009) Effects of glutathione reductase inhibition on cellular thiol redox state and related systems. *Arch Biochem Biophys* **485**, 56-62
42. Franklin, C. C., Backos, D. S., Mohar, I., White, C. C., Forman, H. J., and Kavanagh, T. J. (2009) Structure, function, and post-translational regulation of the catalytic and modifier subunits of glutamate cysteine ligase. *Molecular aspects of medicine* **30**, 86-98
43. Lu, S. C. (2013) Glutathione synthesis. *Biochimica et biophysica acta* **1830**, 3143-3153
44. Grant, C. M., MacIver, F. H., and Dawes, I. W. (1997) Glutathione synthetase is dispensable for growth under both normal and oxidative stress conditions in the yeast Saccharomyces cerevisiae due to an accumulation of the dipeptide gamma-glutamylcysteine. *Molecular Biology of the Cell* **8**, 1699-1707
45. Ristoff, E., Hebert, C., Njalsson, R., Norgren, S., Rooyackers, O., and Larsson, A. (2002) Glutathione synthetase deficiency: is gamma-glutamylcysteine

accumulation a way to cope with oxidative stress in cells with insufficient levels of glutathione? *Journal of inherited metabolic disease* **25**, 577-584

46. Griffith, O. W. (1982) Mechanism of action, metabolism, and toxicity of buthionine sulfoximine and its higher homologs, potent inhibitors of glutathione synthesis. *The Journal of biological chemistry* **257**, 13704-13712
47. Markovic, J., Mora, N. J., Broseta, A. M., Gimeno, A., de-la-Concepción, N., Viña, J., and Pallardó, F. V. (2009) The Depletion of Nuclear Glutathione Impairs Cell Proliferation in 3t3 Fibroblasts. *PLoS ONE* **4**, e6413
48. Vahrmeijer, A. L., van Dierendonck, J. H., Schutrups, J., van de Velde, C. J., and Mulder, G. J. (1999) Effect of glutathione depletion on inhibition of cell cycle progression and induction of apoptosis by melphalan (L-phenylalanine mustard) in human colorectal cancer cells. *Biochemical pharmacology* **58**, 655-664
49. Tomoda, H., Kishimoto, Y., and Lee, Y. C. (1989) Temperature effect on endocytosis and exocytosis by rabbit alveolar macrophages. *The Journal of biological chemistry* **264**, 15445-15450
50. Calton, C. M., Schlegel, A. M., Chapman, J. A., and Campos, S. K. (2013) Human papillomavirus type 16 does not require cathepsin L or B for infection. *J Gen Virol* **94**, 1865-1869
51. Campos, S. K., Chapman, J. A., Deymier, M. J., Bronnimann, M. P., and Ozbun, M. A. (2012) Opposing effects of bacitracin on human papillomavirus type 16 infection: enhancement of binding and entry and inhibition of endosomal penetration. *J Virol* **86**, 4169-4181
52. Sapp, M., Kraus, U., Volpers, C., Snijders, P. J., Walboomers, J. M., and Streeck, R. E. (1994) Analysis of type-restricted and cross-reactive epitopes on virus-like particles of human papillomavirus type 33 and in infected tissues using monoclonal antibodies to the major capsid protein. *J Gen Virol* **75 (Pt 12)**, 3375-3383
53. Spoden, G., Freitag, K., Husmann, M., Boller, K., Sapp, M., Lambert, C., and Florin, L. (2008) Clathrin- and Caveolin-Independent Entry of Human Papillomavirus Type 16—Involvement of Tetraspanin-Enriched Microdomains (TEMs). *PLoS ONE* **3**, e3313
54. Bronnimann, M. P., Calton, C. M., Chiquette, S. F., Li, S., Lu, M., Chapman, J. A., Bratton, K. N., Schlegel, A. M., and Campos, S. K. (2016) Furin Cleavage of L2 During Papillomavirus Infection: Minimal Dependence on Cyclophilins. *J Virol*
55. DiGiuseppe, S., Luszczek, W., Keiffer, T. R., Bienkowska-Haba, M., Guion, L. G., and Sapp, M. J. (2016) Incoming human papillomavirus type 16 genome resides in a vesicular compartment throughout mitosis. *Proc Natl Acad Sci U S A* **113**, 6289-6294
56. MANDERS, E. M. M., VERBEEK, F. J., and ATEN, J. A. (1993) Measurement of co-localization of objects in dual-colour confocal images. *Journal of microscopy* **169**, 375-382
57. Fernandes, A. P., and Holmgren, A. (2004) Glutaredoxins: glutathione-dependent redox enzymes with functions far beyond a simple thioredoxin backup system. *Antioxidants & redox signaling* **6**, 63-74
58. Deponte, M. (2013) Glutathione catalysis and the reaction mechanisms of glutathione-dependent enzymes. *Biochimica et biophysica acta* **1830**, 3217-3266

59. Lash, L. H., Jones, D. P., and Orrenius, S. (1984) The renal thiol (glutathione) oxidase. Subcellular localization and properties. *Biochimica et biophysica acta* **779**, 191-200
60. Lushchak, V. I. (2012) Glutathione homeostasis and functions: potential targets for medical interventions. *Journal of amino acids* **2012**, 736837
61. Lowenstein, C. J., and Tsuda, H. (2006) N-ethylmaleimide-sensitive factor: a redox sensor in exocytosis. *Biol Chem* **387**, 1377-1383
62. Washbourne, P., Cansino, V., Mathews, J. R., Graham, M., Burgoyne, R. D., and Wilson, M. C. (2001) Cysteine residues of SNAP-25 are required for SNARE disassembly and exocytosis, but not for membrane targeting. *The Biochemical journal* **357**, 625-634
63. Kinsella, B. T., and Maltese, W. A. (1991) rab GTP-binding proteins implicated in vesicular transport are isoprenylated in vitro at cysteines within a novel carboxyl-terminal motif. *The Journal of biological chemistry* **266**, 8540-8544
64. Seabra, M. C. (1998) Membrane association and targeting of prenylated Ras-like GTPases. *Cellular signalling* **10**, 167-172
65. Yamaguchi, T., Nakayama, K., Hatsuzawa, K., Tani, K., Himeno, M., and Tagaya, M. (1998) ADP-ribosylation factor-1 is sensitive to N-ethylmaleimide. *Journal of biochemistry* **124**, 1229-1236
66. Grek, C. L., Zhang, J., Manevich, Y., Townsend, D. M., and Tew, K. D. (2013) Causes and consequences of cysteine S-glutathionylation. *The Journal of biological chemistry* **288**, 26497-26504
67. Hess, D. T., Matsumoto, A., Kim, S. O., Marshall, H. E., and Stamler, J. S. (2005) Protein S-nitrosylation: purview and parameters. *Nature reviews. Molecular cell biology* **6**, 150-166
68. DiGiuseppe, S., Bienkowska-Haba, M., Hilbig, L., and Sapp, M. (2014) The nuclear retention signal of HPV16 L2 protein is essential for incoming viral genome to transverse the trans-Golgi network. *Virology* **458-459**, 93-105
69. Boukamp, P., Petrussevska, R. T., Breitkreutz, D., Hornung, J., Markham, A., and Fusenig, N. E. (1988) Normal keratinization in a spontaneously immortalized aneuploid human keratinocyte cell line. *J Cell Biol* **106**, 761-771
70. Campos, S. K., and Ozbun, M. A. (2009) Two highly conserved cysteine residues in HPV16 L2 form an intramolecular disulfide bond and are critical for infectivity in human keratinocytes. *PLoS One* **4**, e4463
71. Schneider, C. A., Rasband, W. S., and Eliceiri, K. W. (2012) NIH Image to ImageJ: 25 years of image analysis. *Nature methods* **9**, 671-675
72. Bolte, S., and Cordelieres, F. P. (2006) A guided tour into subcellular colocalization analysis in light microscopy. *Journal of microscopy* **224**, 213-232
73. McDonald, J. H., and Dunn, K. W. (2013) Statistical tests for measures of colocalization in biological microscopy. *Journal of microscopy* **252**, 295-302